Near-threshold absolute *M*-shell x-ray production cross sections of Au and Bi by electron impact

C. Merlet
CNRS UMR 5243, Université de Montpellier II, GM, Place E. Bataillon, 34095 Montpellier, France

X. Llovet*
Serveis Cientificotècnics, Universitat de Barcelona, Lluís Solé i Sabarís 1-3, 08028 Barcelona, Spain

F. Salvat
Facultat de Física (ECM), Universitat de Barcelona, Diagonal 647, 08028 Barcelona, Spain
(Received 21 May 2008; published 6 August 2008)

Absolute *M*-shell x-ray production cross sections have been measured and calculated for Au and Bi for electron incident energies from close to the ionization threshold up to 38 keV. The experimental cross sections were deduced from $M\alpha$ x-ray intensities emitted from ultrathin Au and Bi samples deposited on self-supporting C films. The measurements were performed on an electron microprobe using several wavelength-dispersive spectrometers. The x-ray production cross sections were also evaluated theoretically using ionization cross sections calculated from the plane-wave and the distorted-wave Born approximations. Experimental results are compared with the calculated cross sections and also with the results of two analytical formulas widely used in many applications. Good agreement is found between the measured cross sections and the predictions from the distorted-wave Born approximation, which indicates that this approximation is suited for the calculation of *M*-shell ionization cross sections of heavy elements.

DOI: 10.1103/PhysRevA.78.022704 PACS number(s): 34.80.Dp

Cross sections for the ionization of inner shells by electron impact are needed for a number of applications, such as electron probe microanalysis, Auger electron spectroscopy, or electron-energy-loss spectroscopy, especially near the ionization threshold [1]. Cross-section data are also required for the characterization of x-ray generators employed in medical and industrial applications and, in general, for the simulation of radiation transport in matter. In spite of these needs, a systematic method to calculate reliable inner-shell ionization cross sections from first principles is not yet readily available. Most quantum-mechanical calculations have been performed by using the plane-wave Born approximation (PWBA), in which the projectile wave functions are described by plane waves. This approximation, however, is not appropriate near the ionization threshold because, at such energies, the distorting effect of the atomic electric field on the projectile wave functions is deemed to be important. In addition, electron exchange effects are important at near-threshold energies and they can only be described approximately within the PWBA [2]. A number of empirical and semiempirical approximate formulas have also been proposed, whose simplicity make them suitable for practical applications, but, unfortunately, they are valid only for certain energy ranges and have limited accuracy [1,3,4].

In recent years, it has become possible to perform systematic calculations of cross sections for inner-shell ionization using the distorted-wave Born approximation (DWBA) [5–7]. The key advantage of this approximation is that the initial and final projectile wave functions are described as distorted plane waves, thus accounting for the distorting effect of the target potential on the projectile wave functions. Moreover, when the orthogonality of the target and projectile electron wave functions is imposed, exchange effects are described consistently. The DWBA, however, neglects correlation effects [8], which may become important for energies close to the ionization threshold. Nevertheless, for the ionization of *K* shells, comparison of calculated cross sections with results of recent accurate measurements indicates that the DWBA provides a good description of the process [9,11,12] (see also Refs. [5–7]). For *L* shells, the situation is less clear, mainly because of the scarcity of experimental data. Furthermore, measured *L*-shell ionization cross sections are generally affected by uncertainties much larger than for *K* shells. The occurrence of (radiationless) Coster-Kronig (CK) transitions between *L* subshells must be taken into consideration when deriving ionization cross sections from measured x-ray production cross sections; uncertainties in the CK transition rates thus propagate to the derived ionization cross section. In spite of this difficulty, comparison of the energy dependence of measured x-ray production cross sections with results from DWBA calculations seems to indicate that this approximation is also well suited for the description of *L*-shell ionization [6,10–12]. However, nothing can be said about the reliability of the DWBA for ionization of *M* shells because of the lack of experimental data to compare against calculations. The few measurements of *M*-shell ionization cross sections described in the literature were either performed at very high electron incident energies [13,14], where the PWBA is supposed to be valid, or were only focused on the energy dependence of the cross section [15–17].

In this study, we present results of measurements of absolute *M*-shell ionization cross sections and we use them to inquire into the reliability of the DWBA for describing the ionization of *M* shells by impact of electrons with energies near the ionization threshold. Specifically, we report absolute

*Author to whom correspondence should be addressed: xavier@sct.ub.es

$M\alpha$ x-ray production cross sections for Au and Bi, for incident electrons from near the ionization threshold up to 38 keV. The measured cross sections are compared with cross sections calculated from the DWBA, as well as with results obtained from the PWBA and with the predictions of two analytical formulas widely used in many applications. For the purpose of this comparison, theoretical M-subshell ionization cross sections have been converted into $M\alpha$ x-ray production cross sections using relaxation parameters, i.e., x-ray emission rates, fluorescence, CK, and super-Coster-Kronig (sCK) yields as well as vacancy-transfer probabilities available from the literature.

The experimental cross sections were obtained by recording $M\alpha$ x-ray intensities emitted from ultrathin Au and Bi samples deposited on self-supporting C films, using a methodology similar to that described in Ref. [12]. Briefly, we assume that electrons penetrate a self-supporting film of the studied element following a straight trajectory without losing energy. This assumption is appropriate for very thin films and/or for electron beams with relatively large energies. The $M\alpha$ x-ray production cross section $\sigma_{M\alpha}$ is given by

$$\sigma_{M\alpha}(E) = \frac{4\pi}{\mathcal{N}tN_e\epsilon\Delta\Omega} N_{M\alpha}(E), \tag{1}$$

where $\mathcal{N}$ is the density of atoms in the target (atoms per unit volume), t is the film thickness, N_e and E are the number and energy of incident electrons, ϵ is the spectrometer efficiency, $\Delta\Omega$ is the solid angle of collection, and $N_{M\alpha}$ is the intensity of the $M\alpha$ line.

The targets were obtained by vacuum evaporation of Au and Bi onto previously prepared ~1.0-$\mu g/cm^2$-thick self-supporting C backing films. During the Au and Bi evaporation runs, high-purity, polished Ta samples were also used as substrates. The resulting "twin" Au/Ta and Bi/Ta samples were utilized to determine the thicknesses of the target films by variable-voltage electron-probe microanalysis (see, e.g., [18]). X-ray intensities of the Au, Bi, and Ta $M\alpha$ lines emitted from the twin Au/Ta and Bi/Ta targets, as well as from bulk reference samples of the mentioned elements, were recorded for electron incident energies from 4 to 30 keV. Figure 1 shows the measured intensity ratios of the Au and Ta $M\alpha$ x-ray lines emitted from a Au/Ta sample with respect to Au and Ta reference samples. An analytical x-ray emission model [21] was used to determine the film thickness by fitting the intensity ratios predicted by the model to the set of measured values. For the Au/Ta sample considered in Fig. 1, the fitted thickness of the Au layer is 3.0 $\mu g/cm^2$. We would like to note that the measured x-ray intensity ratios vary smoothly with energy and that they are in fairly good agreement with the predictions of the x-ray emission model for both the Au and Ta $M\alpha$ lines and for all the incident electron beam energies. From these results, we estimate that the uncertainty of the film thicknesses determined with the x-ray emission model is less than 5%.

For each analyzed element, two different films were used for the cross-section determination. The thinner films, with thicknesses of 0.50 $\mu g/cm^2$ (Au) and 0.67 $\mu g/cm^2$ (Bi), were used to measure x-ray intensities from near the ionization threshold up to 12 keV so as to minimize multiple scattering effects arising from the finite thickness of the active film. These would lead to an artificial increase of the x-ray intensity at low incident energies, as has been shown elsewhere [11]. The thicker films, with thicknesses of 3.0 $\mu g/cm^2$ (Au) and 8.2 $\mu g/cm^2$ (Bi), were used in the measurements for electron energies above 12 keV in order to obtain x-ray intensities with statistical uncertainties less than 1% within reasonable counting times. Results from measurements performed with the two film thicknesses were concatenated and were found to match well at 12 keV.

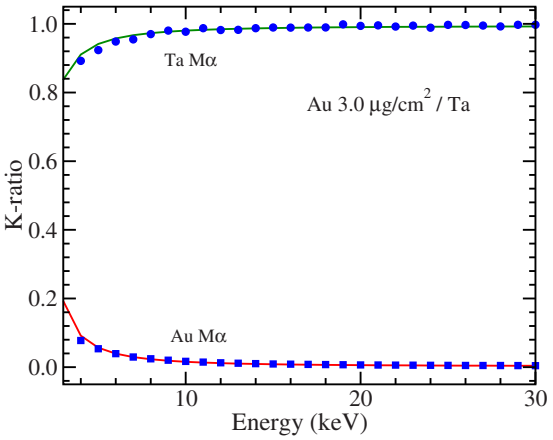

FIG. 1. (Color online) X-ray intensity ratios for the Au and Ta $M\alpha$ lines emitted from a 1.0-$\mu g/cm^2$-thick Au/Ta sample as functions of the incident electron energy. The intensity ratios were determined with respect to pure Au and Ta reference samples. Symbols represent experimental data. Curves are results from Merlet's x-ray emission model [21], which yielded the thickness of this particular target.

All x-ray measurements were performed on a CAMECA SX-100 electron microprobe, using several wavelength-dispersive (WD) spectrometers. These are oriented so as to collect x rays that emerge in directions forming an angle of 40° with the sample surface and contain up to four different dispersing crystals and one Ar-CH_4 flow proportional counter. After being diffracted by the crystals, the x rays are detected on the proportional counter and recorded with a pulse-height analyzer.

A typical $M\alpha_{1,2}$ x-ray spectrum emitted from a Bi 8.2 $\mu g/cm^2$–C 1.0 $\mu g/cm^2$ sample bombarded with 20-keV electrons is displayed in Fig. 2. The observed parent lines originate from the filling of vacancies in the M_5 shells due to transitions of electrons from N_6 ($M\alpha_1$) and N_7 ($M\alpha_2$) shells. In the high-energy tail of the $M\alpha_1$ line are satellite lines arising from the decay of double-vacancy states that can be created by shake-off, Auger, CK, and sCK transitions [22]. Measured spectra were fitted with a weighted sum of pseudo-Voigt profiles, one for each line in the spectrum (see, e.g., Ref. [20]). To improve the accuracy of measured x-ray intensities, the profiles were determined from the fitted spectrum, as described in Ref. [19].

The x-ray intensities were recorded from 2.5 to 38 keV in steps of, at most, 1 keV. The electron current was 100 nA in all measurements. For each accelerating voltage, measurements were performed at more than ten different positions,

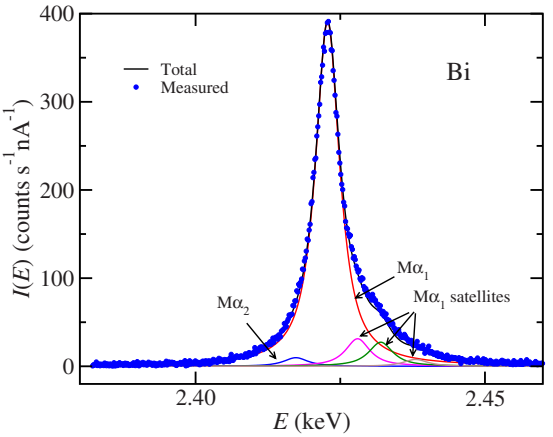

FIG. 2. (Color online) Typical x-ray spectrum emitted from a Bi 8.2 $\mu g/cm^2$–C 0.3 $\mu g/cm^2$ sample, recorded with a LPET crystal. Symbols represent the measured spectrum; the continuous curve is the sum of the fitted $M\alpha_1$ and $M\alpha_2$ peaks and satellite peaks.

on five different self-supporting films, and with typical counting times of 600 s. Intensities were recorded simultaneously by using three spectrometers with PET (pentaerythritol) and LPET (large pentaerythritol) crystals, and the results were averaged to give the "measured" intensity. The number of incident electrons was estimated by multiplying the reading of the electron current by the acquisition time.

The efficiency of the WD spectrometers was determined by combining Monte Carlo simulation with measurements of bremsstrahlung intensities (N_i) at wavelength channels corresponding to the Au $M\alpha$ and Bi $M\alpha$ peaks on a C reference sample at an incident electron energy of 6 keV. Carbon was chosen as the reference material because neither absorption edges nor spectral lines could be observed in a wide wavelength interval around the wavelengths of interest. In addition, its low backscattering coefficient ensures minimal production of stray radiation. Measurements were performed at 10 different sample positions, with counting times long enough to ensure that the statistical uncertainties were less than 1%. The corresponding theoretical bremsstrahlung spectrum $N(E)$ was calculated using the general-purpose Monte Carlo simulation code PENELOPE [23]. The product of the spectrometer efficiency times the solid angle of collection, $\epsilon\Delta\Omega$, evaluated at the wavelength channel corresponding to $\lambda_i = hc/E_i$, was obtained from the relation [19]

$$\epsilon(\lambda_i)\Delta\Omega = \frac{N_i\Delta\lambda}{\int_{E(\lambda_i+\Delta\lambda)}^{E(\lambda_i)} N(E)\mathrm{d}E}, \tag{2}$$

where $N(E)\mathrm{d}E$ is the theoretical number of bremsstrahlung photons with energies between E and $E+\mathrm{d}E$, per incident electron, emitted from the C reference sample, $\Delta\lambda$ is the width of the wavelength channel, and N_i is the experimental number of photons detected at the channel $(\lambda_i, \lambda_i+\Delta\lambda)$ per incident electron.

Experimental cross sections are affected by random uncertainties mainly arising from counting statistics, sample nonuniformity, stray radiation, and instrumental drift. From repeated measurements, random uncertainties were estimated to be less than 1%, except very close to the ionization threshold, where uncertainties are larger due to the low x-ray intensities. Conversion of x-ray intensities to absolute cross sections introduces uncertainties of a systematic nature. These uncertainties are essentially the same for all incident electron energies, and therefore they produce a global shift of the cross section versus energy curves, without affecting their shape. Systematic uncertainties come from the adopted values for the target thickness (5%), number of incident electrons (2%), and detector efficiency (10%). The global uncertainties, obtained by combining random and systematic contributions in quadrature, were ~11%.

Electron-impact ionization cross sections for all the L and M subshells of Au and Bi were calculated using the PWBA, the DWBA, the empirical formula of Casnati *et al.* [24], and Gryzinski's semiclassical model [25]. The PWBA and DWBA cross sections were obtained by using the codes developed by Bote and Salvat [7]. To allow direct comparison with our experimental measurements, $M\alpha$ x-ray production cross sections were derived from the calculated M-subshell ionization cross sections. In the energy range considered here, 2.5–38 keV, vacancies in the M_5 subshell of Au and Bi are produced by direct electron impact, by CK and sCK transitions, and by radiative and nonradiative transitions for vacancies of the L subshells to the M_5 subshell. The cross section for the production of $M\alpha$ x rays, $\sigma_{M\alpha}$, has been evaluated as

$$\begin{aligned}\sigma_{M\alpha} = \frac{\Gamma_{M_5N_{6,7}}}{\Gamma_{M_5\mathrm{Total}}}\omega_{M_5}\{&\sigma_{M_5} + \sigma_{M_4}f_{45} + \sigma_{M_3}(S_{35} + S_{34}f_{45}) \\ &+ \sigma_{M_2}[S_{25} + S_{23}S_{35} + f_{45}(S_{24} + S_{23}S_{34})] \\ &+ \sigma_{M_1}[S_{15} + S_{12}S_{25} + S_{13}S_{35} + S_{12}S_{23}S_{35} \\ &+ f_{45}(S_{14} + S_{12}S_{24} + S_{13}S_{34} + S_{12}S_{23}S_{34})] \\ &+ \sigma_{L_3}n_{L_3M_5} + \sigma_{L_2}n_{L_2M_5} + \sigma_{L_1}n_{L_1M_5}\},\end{aligned} \tag{3}$$

where $\Gamma_{M_5N_{6,7}}$ and $\Gamma_{M_5\mathrm{Total}}$ are the x-ray emission rates for the transition $M_5N_{6,7}$ and for all possible transitions to the M_5 subshell, respectively. ω_{M_5} is the fluorescence yield for the M_5 subshell, σ_{M_i} and σ_{L_i} are the cross sections for the ionization of the M_i and L_i subshells, respectively. f_{45} is the CK yield between the M_4 and M_5 subshells; S_{ji} are yields for sCK transitions $M_i \rightarrow M_j$ between the M subshells indicated by the subscripts. Finally, $n_{L_1M_5}$, $n_{L_2M_5}$, and $n_{L_3M_5}$ are the radiative plus nonradiative yields for transitions of vacancies from the L_1, L_2, and L_3 subshells to the M_5 subshell (the contribution from additional vacancies produced through CK transitions of the type $L_iL_jM_5$ is negligible).

For the shells and transitions considered in this study, the required relaxation data are available from the theoretical calculations of Bhalla [26], McGuire [27], and Chen *et al.* [28] (fitted values to McGuire's calculations are also given in Ref. [29]) and they can also be extracted from the Evaluated Atomic Data Library (EADL) [30]. As indicated above, relaxation parameters are affected by sizeable uncertainties, which propagate to the calculated x-ray production cross sections. Indeed, for a given set of theoretical M-subshell ion-

TABLE I. M_5-subshell fluorescence, CK, and sCK yields adopted in this work [30].

	ω_{M_5}	f_{45}	S_{12}	S_{13}	S_{14}	S_{15}	S_{23}	S_{24}	S_{25}	S_{34}	S_{35}
Au	0.0298	0.0665	0.1258	0.5950	0.0806	0.1111	0.0884	0.5761	0.0926	0.0723	0.6047
Bi	0.0373	0.0606	0.1180	0.5983	0.0835	0.1141	0.0876	0.5803	0.0922	0.0799	0.5919

ization cross sections, the $M\alpha$ x-ray production cross sections obtained by using relaxation data from the various available sources were found to lie within an "uncertainty band" whose width is ~10% for Au and ~12% for Bi. It is worth pointing out that the various sets of relaxation data yield x-ray production cross sections that, when plotted as functions of the electron beam energy, have essentially the same shape (in other words, their ratios are nearly constant with energy). In order to allow comparison with experiment, we have adopted relaxation parameters extracted from the EADL [30], which are summarized in Tables I and II.

The x-ray production cross sections resulting from our measurements are displayed in Fig. 3 as functions of the incident electron energy E, where representative absolute uncertainties are indicated by error bars. Figure 3 also displays theoretical x-ray production cross sections derived from impact-ionization cross sections obtained from the PWBA, the DWBA, the empirical formula of Casnati *et al.* [24], and Gryzinski's semiclassical model [25] using relaxation data extracted from the EADL [30]. The measured cross sections, as well as the required subshell ionization cross sections obtained from the DWBA for Au and Bi, are collected in Tables III and IV, respectively.

In the case of Au, the DWBA calculations are seen to be in excellent agreement with our measurements both in relative and absolute terms. In contrast, the PWBA model lies ~4% above our experimental values, whereas the formulas of Casnati *et al.* and Gryzinski are ~18% and ~25% lower, respectively, than our measurements. For Bi, the energy dependence of the DWBA cross section shows good agreement with the measured values, but the predictions of the DWBA are about 7% higher than the experimental data. Note that differences between the DWBA cross sections and the measurements are less than experimental uncertainties. For this element, PWBA calculations are about 10% higher than the experimental data, whereas the formulas of Casnati *et al.* and Gryzinski are ~10% and ~20% lower, respectively, than our measurements.

It is interesting to note that the shapes of the $\sigma_{M\alpha}(E)$ versus electron energy curves obtained from the DWBA are in close agreement with our measurements. The cross section resulting from the formula of Casnati *et al.* has its maximum at nearly the correct position, but decreases too slowly when the electron energy increases. The PWBA and the Gryzinski formula predict cross sections with the maximum shifted to higher energies, and the Gryzinski cross section decreases somewhat more slowly than the DWBA cross section.

In conclusion, we have performed measurements of the $M\alpha$ x-ray production cross section of Au and Bi, for electrons with kinetic energies from 2.5 keV up to 38 keV, with global uncertainties of ~11%. We have shown that the predictions of the DWBA [7], combined with relaxation data extracted from the EADL [30], are in excellent agreement, both in relative and absolute terms, with our measurements for Au. In the case of Bi, the DWBA-EADL cross sections

TABLE II. X-ray emission rate and radiative plus nonradiative probabilities for transitions of vacancies from the L subshells to the M_5 subshell adopted in this work [30]. Note that $n_{L_1M_5}=0$.

	$\Gamma_{M_5N_{6,7}}/\Gamma_{M_5\text{total}}$	$n_{L_2M_5}$	$n_{L_3M_5}$
Au	0.9319	0.1850	0.6051
Bi	0.9491	0.1608	0.6022

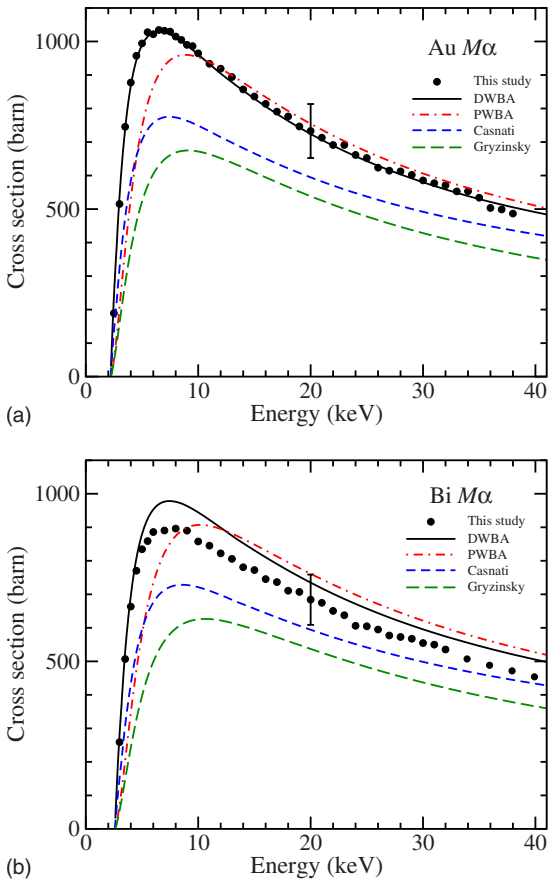

FIG. 3. (Color online) Absolute $M\alpha$ x-ray production cross sections vs incident electron energy for Au (a) and Bi (b). Full circles are the present measurements. Solid and dot-dashed curves are the present DWBA and PWBA calculations, respectively; short- and long-dashed curves indicate the results from the formulas of Casnati *et al.* and Gryzinski, respectively. The plotted uncertainty bars represent the global uncertainties of the present measurements (for the sake of visual clarity, they are only displayed at one incident electron energy).

TABLE III. Measured $M\alpha$ x-ray production cross sections and theoretical *M*- and *L*-subshell ionization cross sections calculated within the DWBA for Au (in barn). Note that 1.708[+1] means 1.708×10^1.

		Calculated cross sections (DWBA)							
E (keV)	Measured $\sigma_{M\alpha}$	σ_{M_1}	σ_{M_2}	σ_{M_3}	σ_{M_4}	σ_{M_5}	σ_{L_1}	σ_{L_2}	σ_{L_3}
2.5	189				3.532[+3]	8.224[+3]			
3.0	515			1.961[+3]	9.713[+3]	1.752[+4]			
3.5	745	1.808[+2]	7.941[+2]	4.543[+3]	1.327[+4]	2.274[+4]			
4.0	877	9.340[+2]	1.574[+3]	6.207[+3]	1.531[+4]	2.567[+4]			
4.5	957	1.455[+3]	2.099[+3]	7.314[+3]	1.649[+4]	2.733[+4]			
5.0	994	1.812[+3]	2.463[+3]	8.057[+3]	1.715[+4]	2.820[+4]			
5.5	1028	2.054[+3]	2.719[+3]	8.556[+3]	1.748[+4]	2.860[+4]			
6.0	1021	2.221[+3]	2.895[+3]	8.891[+3]	1.762[+4]	2.872[+4]			
6.5	1034	2.334[+3]	3.019[+3]	9.108[+3]	1.762[+4]	2.864[+4]			
7.0	1032	2.408[+3]	3.105[+3]	9.241[+3]	1.754[+4]	2.843[+4]			
7.5	1030	2.456[+3]	3.164[+3]	9.310[+3]	1.739[+4]	2.812[+4]			
8.0	1015	2.484[+3]	3.202[+3]	9.333[+3]	1.720[+4]	2.776[+4]			
8.5	1005	2.496[+3]	3.223[+3]	9.320[+3]	1.697[+4]	2.737[+4]			
9.0	990	2.497[+3]	3.232[+3]	9.281[+3]	1.674[+4]	2.696[+4]			
9.5	986	2.491[+3]	3.230[+3]	9.222[+3]	1.649[+4]	2.653[+4]			
10.0	965	2.477[+3]	3.221[+3]	9.148[+3]	1.624[+4]	2.610[+4]			
11.0	934	2.439[+3]	3.187[+3]	8.967[+3]	1.573[+4]	2.524[+4]			
12.0	919	2.391[+3]	3.137[+3]	8.761[+3]	1.524[+4]	2.440[+4]			1.145[+1]
13.0	894	2.337[+3]	3.078[+3]	8.543[+3]	1.475[+4]	2.360[+4]			1.357[+2]
14.0	857	2.282[+3]	3.015[+3]	8.321[+3]	1.429[+4]	2.284[+4]		9.631[+0]	2.321[+2]
15.0	836	2.227[+3]	2.949[+3]	8.101[+3]	1.386[+4]	2.213[+4]	1.708[+1]	4.749[+1]	3.073[+2]
16.0	814	2.173[+3]	2.882[+3]	7.886[+3]	1.345[+4]	2.145[+4]	3.893[+1]	7.798[+1]	3.666[+2]
17.0	791	2.120[+3]	2.816[+3]	7.678[+3]	1.306[+4]	2.081[+4]	5.697[+1]	1.027[+2]	4.136[+2]
18.0	776	2.069[+3]	2.751[+3]	7.477[+3]	1.269[+4]	2.021[+4]	7.198[+1]	1.228[+2]	4.512[+2]
19.0	747	2.020[+3]	2.688[+3]	7.285[+3]	1.234[+4]	1.965[+4]	8.458[+1]	1.394[+2]	4.814[+2]
20.0	733	1.972[+3]	2.626[+3]	7.102[+3]	1.202[+4]	1.912[+4]	9.521[+1]	1.530[+2]	5.057[+2]
21.0	713	1.928[+3]	2.567[+3]	6.927[+3]	1.171[+4]	1.862[+4]	1.042[+2]	1.642[+2]	5.253[+2]
22.0	691	1.885[+3]	2.510[+3]	6.760[+3]	1.142[+4]	1.815[+4]	1.119[+2]	1.736[+2]	5.411[+2]
23.0	691	1.844[+3]	2.455[+3]	6.600[+3]	1.114[+4]	1.771[+4]	1.185[+2]	1.814[+2]	5.539[+2]
24.0	661	1.804[+3]	2.403[+3]	6.449[+3]	1.088[+4]	1.729[+4]	1.241[+2]	1.879[+2]	5.642[+2]
25.0	652	1.767[+3]	2.352[+3]	6.304[+3]	1.063[+4]	1.689[+4]	1.290[+2]	1.934[+2]	5.724[+2]
26.0	624	1.731[+3]	2.304[+3]	6.167[+3]	1.040[+4]	1.651[+4]	1.331[+2]	1.980[+2]	5.789[+2]
27.0	615	1.696[+3]	2.258[+3]	6.036[+3]	1.018[+4]	1.615[+4]	1.367[+2]	2.018[+2]	5.840[+2]
28.0	613	1.664[+3]	2.214[+3]	5.911[+3]	9.964[+3]	1.581[+4]	1.398[+2]	2.050[+2]	5.878[+2]
29.0	602	1.632[+3]	2.171[+3]	5.792[+3]	9.764[+3]	1.549[+4]	1.425[+2]	2.076[+2]	5.907[+2]
30.0	586	1.602[+3]	2.131[+3]	5.678[+3]	9.572[+3]	1.518[+4]	1.448[+2]	2.097[+2]	5.927[+2]
31.0	577	1.573[+3]	2.092[+3]	5.569[+3]	9.389[+3]	1.489[+4]	1.468[+2]	2.115[+2]	5.939[+2]
32.0	571	1.546[+3]	2.054[+3]	5.465[+3]	9.214[+3]	1.460[+4]	1.485[+2]	2.129[+2]	5.945[+2]
33.0	553	1.519[+3]	2.018[+3]	5.366[+3]	9.046[+3]	1.433[+4]	1.499[+2]	2.140[+2]	5.945[+2]
34.0	553	1.494[+3]	1.984[+3]	5.270[+3]	8.885[+3]	1.408[+4]	1.511[+2]	2.149[+2]	5.941[+2]
35.0	534	1.469[+3]	1.951[+3]	5.179[+3]	8.732[+3]	1.383[+4]	1.522[+2]	2.156[+2]	5.933[+2]
36.0	503	1.445[+3]	1.919[+3]	5.092[+3]	8.587[+3]	1.361[+4]	1.530[+2]	2.161[+2]	5.921[+2]
37.0	499	1.423[+3]	1.888[+3]	5.007[+3]	8.449[+3]	1.339[+4]	1.537[+2]	2.164[+2]	5.907[+2]
38.0	487	1.401[+3]	1.858[+3]	4.927[+3]	8.320[+3]	1.319[+4]	1.543[+2]	2.165[+2]	5.890[+2]

TABLE IV. Measured $M\alpha$ x-ray production cross sections and theoretical M- and L-subshell ionization cross sections calculated within the DWBA for Bi (in barn). Note that 1.708[+1] means 1.708×10^{1}.

E (keV)	Measured $\sigma_{M\alpha}$	Calculated cross sections (DWBA)							
		σ_{M_1}	σ_{M_2}	σ_{M_3}	σ_{M_4}	σ_{M_5}	σ_{L_1}	σ_{L_2}	σ_{L_3}
3.0	259				3.531[+3]	7.766[+3]			
3.5	507			1.661[+3]	7.416[+3]	1.353[+4]			
4.0	664	3.277[+1]	4.649[+2]	3.393[+3]	9.755[+3]	1.694[+4]			
4.5	770	5.655[+2]	1.015[+3]	4.553[+3]	1.118[+4]	1.898[+4]			
5.0	835	9.480[+2]	1.397[+3]	5.355[+3]	1.205[+4]	2.020[+4]			
5.5	859	1.221[+3]	1.670[+3]	5.920[+3]	1.259[+4]	2.092[+4]			
6.0	886	1.417[+3]	1.869[+3]	6.317[+3]	1.290[+4]	2.132[+4]			
7.0	890	1.655[+3]	2.123[+3]	6.793[+3]	1.313[+4]	2.152[+4]			
8.0	896	1.776[+3]	2.260[+3]	7.011[+3]	1.306[+4]	2.129[+4]			
9.0	890	1.831[+3]	2.331[+3]	7.080[+3]	1.284[+4]	2.087[+4]			
10.0	858	1.847[+3]	2.360[+3]	7.058[+3]	1.256[+4]	2.034[+4]			
11.0	845	1.842[+3]	2.363[+3]	6.982[+3]	1.224[+4]	1.978[+4]			
12.0	822	1.822[+3]	2.348[+3]	6.872[+3]	1.191[+4]	1.922[+4]			
13.0	806	1.795[+3]	2.323[+3]	6.743[+3]	1.158[+4]	1.866[+4]			
14.0	781	1.763[+3]	2.291[+3]	6.602[+3]	1.126[+4]	1.812[+4]			5.517[+1]
15.0	772	1.729[+3]	2.254[+3]	6.457[+3]	1.095[+4]	1.760[+4]			1.351[+2]
16.0	745	1.694[+3]	2.214[+3]	6.310[+3]	1.065[+4]	1.710[+4]		6.767[+0]	1.989[+2]
17.0	736	1.658[+3]	2.173[+3]	6.164[+3]	1.037[+4]	1.663[+4]	1.106[+1]	3.267[+1]	2.502[+2]
18.0	711	1.624[+3]	2.131[+3]	6.021[+3]	1.010[+4]	1.619[+4]	2.644[+1]	5.407[+1]	2.917[+2]
19.0	707	1.589[+3]	2.090[+3]	5.882[+3]	9.843[+3]	1.576[+4]	3.941[+1]	7.183[+1]	3.255[+2]
20.0	684	1.556[+3]	2.048[+3]	5.747[+3]	9.599[+3]	1.536[+4]	5.042[+1]	8.666[+1]	3.532[+2]
21.0	675	1.524[+3]	2.008[+3]	5.617[+3]	9.367[+3]	1.498[+4]	5.982[+1]	9.910[+1]	3.758[+2]
22.0	650	1.493[+3]	1.968[+3]	5.492[+3]	9.147[+3]	1.462[+4]	6.789[+1]	1.096[+2]	3.945[+2]
23.0	638	1.463[+3]	1.930[+3]	5.372[+3]	8.938[+3]	1.428[+4]	7.485[+1]	1.184[+2]	4.100[+2]
24.0	606	1.435[+3]	1.892[+3]	5.257[+3]	8.738[+3]	1.395[+4]	8.087[+1]	1.259[+2]	4.228[+2]
25.0	605	1.407[+3]	1.856[+3]	5.146[+3]	8.549[+3]	1.365[+4]	8.609[+1]	1.323[+2]	4.335[+2]
26.0	595	1.380[+3]	1.821[+3]	5.041[+3]	8.369[+3]	1.335[+4]	9.063[+1]	1.377[+2]	4.423[+2]
27.0	577	1.355[+3]	1.788[+3]	4.939[+3]	8.197[+3]	1.307[+4]	9.462[+1]	1.424[+2]	4.495[+2]
28.0	573	1.330[+3]	1.755[+3]	4.842[+3]	8.033[+3]	1.281[+4]	9.810[+1]	1.464[+2]	4.554[+2]
29.0	568	1.307[+3]	1.724[+3]	4.749[+3]	7.876[+3]	1.255[+4]	1.012[+2]	1.498[+2]	4.602[+2]
30.0	555	1.284[+3]	1.693[+3]	4.660[+3]	7.727[+3]	1.231[+4]	1.038[+2]	1.527[+2]	4.640[+2]
31.0	550	1.262[+3]	1.664[+3]	4.575[+3]	7.584[+3]	1.208[+4]	1.062[+2]	1.552[+2]	4.670[+2]
32.0	535	1.241[+3]	1.636[+3]	4.493[+3]	7.447[+3]	1.186[+4]	1.082[+2]	1.573[+2]	4.694[+2]

reproduce the shape of the experimental cross-section curve well, but they overestimate the magnitude of measured values by ~7%. Nonetheless, the uncertainties in the relaxation parameters required for calculating the M x-ray production cross sections make it difficult to draw a definite conclusion about the reliability of the DWBA calculations for M shells. More experimental information on M-shell ionization cross sections of other elements is required as well for a more definite assessment of the reliability of the DWBA.

We would like to thank David Bote for providing us with the DWBA and PWBA numerical data. This work has been partially supported by the Spanish Ministerio de Educación y Ciencia, project no. FPA2006-12066, and by the AGAUR, Generalitat de Catalunya (SGR 00013).

[1] C. J. Powell, in *Electron Impact Ionization*, edited by T. D. Märk and D. H. Dunn (Springer-Verlag, Berlin, 1985), Chap. 6.
[2] S. Segui, M. Dingfelder, J. M. Fernández-Varea, and F. Salvat, J. Phys. B **35**, 33 (2002).
[3] C. J. Powell, Rev. Mod. Phys. **48**, 33 (1976).
[4] C. J. Powell, in *Microbeam Analysis*, edited by J. R. Michael and P. Ingram (San Francisco Press, San Francisco, 1990).
[5] S. Segui, M. Dingfelder, and F. Salvat, Phys. Rev. A **67**, 062710 (2003).
[6] J. Colgan, C. J. Fontes, and H. L. Zhang, Phys. Rev. A **73**, 062711 (2006).
[7] D. Bote and F. Salvat, Phys. Rev. A **77**, 042701 (2008).
[8] S. Jones and D. H. Madison, Phys. Rev. Lett. **81**, 2886 (1998).
[9] X. Llovet, C. Merlet, and F. Salvat, J. Phys. B **35**, 973 (2002).
[10] C. S. Campos, M. A. Z. Vasconcellos, X. Llovet, and F. Salvat, Phys. Rev. A **66**, 012719 (2002).
[11] C. Merlet, X. Llovet, and F. Salvat, Phys. Rev. A **69**, 032708 (2004).
[12] C. Merlet, X. Llovet, and J. M. Fernández-Varea, Phys. Rev. A **73**, 062719 (2006); **74**, 049901(E) (2006).
[13] K. Ishii, M. Kamiya, K. Sera, and S. Morita, Phys. Rev. A **15**, 906 (1977).
[14] D. H. H. Hoffmann, C. Brendel, H. Genz, W. Low, S. Muller, and A. Richter, Z. Phys. A **293**, 187 (1979).
[15] H. Berndt and H. J. Hunger, Phys. Status Solidi A **84**, K149 (1984).
[16] K. Murata and K. Sugiyama, J. Appl. Phys. **66**, 4456 (1989).
[17] X. Llovet, C. Merlet, J. M. Fernández-Varea, and F. Salvat, Mikrochim. Acta **132**, 163 (2000).
[18] A. P. Mackenzie, Rep. Prog. Phys. **56**, 557 (1993).
[19] C. Merlet and X. Llovet, Microchim. Acta **155**, 199 (2006).
[20] C. Fournier, C. Merlet, O. Dugne, and M. Fialin, J. Anal. At. Spectrom. **14**, 381 (1999).
[21] C. Merlet, in *Proceedings, Microbeam Analysis*, edited by E. S. Etz (VHC, New York, 1995), p. 203.
[22] A. M. Vlaicu, Y. Ito, K. Taniguchi, T. Mukoyama, and T. Bastug, Radiat. Phys. Chem. **61**, 401 (2001).
[23] F. Salvat, J. M. Fernández-Varea, and J. Sempau, PENELOPE-2006: *A Code System For Monte Carlo Simulation of Electron and Photon Transport* (OECD/NEA Data Bank, Issy-les-Moulineaux, France, 2006).
[24] E. Casnati, A. Tartari, and C. Baraldi, J. Phys. B **15**, 155 (1982).
[25] M. Gryzinski, Phys. Rev. **138**, A336 (1965).
[26] C. P. Bhalla, J. Phys. B **3**, 916 (1970).
[27] E. J. McGuire, Phys. Rev. A **5**, 1043 (1972).
[28] M. H. Chen, B. Crasemann, and H. Märk, Phys. Rev. A **21**, 449 (1980).
[29] Ö. Söğüt, E. Büyükkasap, A. Küçükönder, M. Ertuğrul, O. Doğan, H. Erdoğan, and Ö. Şimşek, X-Ray Spectrom. **31**, 62 (2002).
[30] S. T. Perkins, D. E. Cullen, M. H. Chen, J. H. Hubbell, J. Rath, and J. Scofield, Report UCRL-50400 30, Lawrence Livermore National Laboratory, Livermore, CA, 1991.